

# RSC Advances



This is an *Accepted Manuscript*, which has been through the Royal Society of Chemistry peer review process and has been accepted for publication.

*Accepted Manuscripts* are published online shortly after acceptance, before technical editing, formatting and proof reading. Using this free service, authors can make their results available to the community, in citable form, before we publish the edited article. This *Accepted Manuscript* will be replaced by the edited, formatted and paginated article as soon as this is available.

You can find more information about *Accepted Manuscripts* in the [Information for Authors](#).

Please note that technical editing may introduce minor changes to the text and/or graphics, which may alter content. The journal's standard [Terms & Conditions](#) and the [Ethical guidelines](#) still apply. In no event shall the Royal Society of Chemistry be held responsible for any errors or omissions in this *Accepted Manuscript* or any consequences arising from the use of any information it contains.

## PAPER

# Enhancement of Long Stability of Li-S battery by Thin Wall Hollow Spherical Structured Polypyrrole Based Sulfur Cathode

Cite this: DOI: 10.1039/x0xx00000x

Received 00th January 2012,  
Accepted 00th January 2012

DOI: 10.1039/x0xx00000x

www.rsc.org/

Guoqiang Ma<sup>a</sup>, Zhaoyin Wen<sup>\*a</sup>, Jun Jin<sup>a</sup>, Yan Lu<sup>a</sup>, Xiangwei Wu<sup>a</sup>, Cai Liu<sup>a</sup>,  
Chunhua Chen<sup>b</sup>

To enhance the long stability of sulfur cathode for a high energy lithium-sulfur cell, thin wall hollow spherical structured polypyrrole (T-HSSP) composed of a mono layer of PPy nanoparticles is employed as the host to encapsulate sulfur component. T-HSSP can buffer the volume expansion sulfur during discharge and charge processes, and therefore fully keep the integrity of the sulfur electrode after long cycling. Distribution of sulfur component is well remained even after 100 charge/discharge cycles in T-HSSP, indicating efficient effect of the design in inhibiting the shuttle effect of the sulfur electrode. The composite with a sulfur content of 58.4 wt.% exhibits a reversible capacity of 1563.3 mAh.g<sup>-1</sup> and a discharge capacity retention over 89% during 40-200 cycles corresponding to a sulfur utilization of 89.2% at 0.2C. Excellent rate capability of the composite demonstrated by its cycling performances at 1C, 2C and 5C for 300 cycles. Moreover, a further heating treatment is carried out to inhibit the severe capacity fade in the initial tens of cycles, and an enhanced cycling stability of Li-S battery is achieved.

## Introduction

Among various types of rechargeable batteries, Li-S battery has attracted great attentions due to its high theoretical specific capacity (1675mAh.g<sup>-1</sup>) and energy density (2600Wh.Kg<sup>-1</sup>). These values are several times greater than those of common lithium-ion batteries<sup>1, 2</sup>. In combination with the natural abundance, low cost and environmental friendliness of sulfur, the Li-S battery becomes a promising candidate for the next generation power sources.

However, the development of Li-S battery has encountered the following disadvantages. Firstly, the insulating nature of sulfur (5×10<sup>-30</sup> S.cm<sup>-1</sup> at 25 °C) leads to a low utilization rate of active material and a poor high-rate capability. Secondly, the lithium polysulfides generated during the electrochemical-reduction process are highly soluble in conventional organic electrolytes, and would easily reach the Li anode to cause immediate reaction with the metallic lithium with the formation of insulating Li<sub>2</sub>S. This results in serious anode corrosion and a redistribution of sulfur component in the electrode<sup>3-5</sup>. The so called shuttle mechanism is the major reason for the low coulombic efficiency and the poor cycling ability of lithium sulfur cells<sup>6-9</sup>. Thirdly, volume change of sulfur as high as 80% during the charge/discharge process destroys the electrode structure and integrity of the cell, leading to a serious capacity fading and finally a short life of the cell<sup>10, 11</sup>.

Various approaches including the modification of cathode<sup>12</sup>, electrolyte<sup>13, 14</sup>, separator<sup>15</sup>, and Li-metal anode<sup>16, 17</sup> have been

adopted to improve the cycling ability by different research teams world-wide. Among them, the fabrication of sulfur cathode with a unique structure is most widely adopted. Normally, sulfur is embedded in the conductive carbon matrix to increase the conductivity of sulfur cathode and suppress the shuttle effect. Carbon materials like active carbon<sup>12, 18</sup>, mesoporous carbon<sup>19-21</sup>, microporous carbon<sup>22-25</sup>, carbon nanotube<sup>26-28</sup>, graphene<sup>28-30</sup>, hollow carbon fibers<sup>31, 32</sup>, TiO<sub>2</sub><sup>33</sup> and conductive polymers<sup>29, 34-37</sup> have been applied to achieve such purposes. Wrapping sulfur nano-particles with carbon<sup>38-40</sup>, and conductive polymers<sup>41-43</sup> is also frequently taken as an alternative route to improve the conductivity of sulfur electrode and at the same time to inhibit the dissolution of lithium polysulfides in electrolyte. However, all these attempts are less effective in buffering the serious volume change during cycling. Recently, a yolk-shell microstructure of sulfur-TiO<sub>2</sub> and a hollow structured sulfur coated with PEDOT are reported<sup>10, 11</sup>. Such a approach is found to improve the conductivity of the sulfur cathode and inhibit the shuttle effect simultaneously. Further buffering the volume expansion by the void space of the sulfur during the charge/discharge process, resulting in an excellent prolonged cycling stability.

Conducting polymeric matrices are known to allow better accommodation of volume expansion than pure carbon<sup>8, 44</sup>. Polypyrrole (PPy) is electrochemically active in the voltage range of 2-4 V vs. Li/Li<sup>+</sup><sup>45</sup>, and hence it is widely used in various high energy density battery systems such as Li-ion battery<sup>46, 47</sup>, Li-S battery<sup>43, 48</sup>, and Li-air<sup>45, 49</sup> etc. Recently, PPy

hollow sphere has been employed as the matrix of sulfur<sup>50</sup>, however, the hollow volume in the PPy hollow spheres is not large enough to load more sulfur and buffer volume expansion and the thick shell hinders migration of  $\text{Li}^+$  and electrons, in addition to low heating treatment temperature, so the cycling performance is unsatisfactory even with low sulfur loading. In the present study, thin wall hollow spherical structured polypyrrole (T-HSSP) is quantitatively designed to supply enough void space for the lithiation of sulfur. T-HSSP have outer diameter of about 300nm and shell thickness of about 30nm, which are composed of a mono layer of PPy nanoparticles with diameter in the range of 25-35nm. As indicated in Fig. 1a, the thin wall of T-HSSP is beneficial for both electron transport and  $\text{Li}^+$  diffusion. Moreover, the dissolution of sulfur entrapped in the T-HSSP is almost completely inhibited by the wall. The potential S-C bond generated during heating treatment can further inhibit the shuttle effect during charge/discharge process. Furthermore, volume expansion during charge/discharge process could be fully buffered by the void space in the T-HSSP. Consequently, the dimension of the T-HSSP will be retained after cycling, leading to integrity of the sulfur electrode and excellent cell performance as schematically illustrated in Fig. 1b.

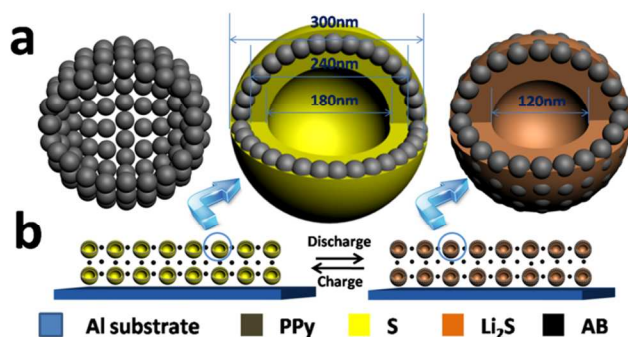


**Fig. 1** (a) Schematic of T-HSSP, S@PPy composite and lithiated (discharged) S@PPy composite with inward expansion of the sulfur entrapped in the hollow sphere, (b) Schematic illustration of integrity of the T-HSSP-based sulfur electrode with serious expansion during discharge and charge processes.

## Experimental

### Preparation of T-HSSP

T-HSSP were synthesized by a modified template process over the initial one proposed in the literature<sup>51</sup>, for which the  $\text{SiO}_2$  nanoparticles were firstly synthesized by the traditional base-catalyzed hydrolysis of TEOS<sup>52</sup>. As a typical example, 12 ml of aqueous ammonia (25 wt. %) was added into a solution containing 260 ml of ethanol and 40 ml of deionized water. Separately, 24 ml of TEOS was mixed with 40 ml of ethanol. The two solutions were rapidly mixed under vigorous stirring for 2 h to allow the formation of uniform silica particles. Then, the resulting silica particles were separated by centrifugation at 8000 rpm for 10 min and washed several times with water and ethanol.

Consequently, the obtained  $\text{SiO}_2$  microspheres were dispersed in 500 mL deionized water by ultrasound for 30 minutes. Subsequently, 10g Poly(vinyl pyrrolidone) (PVP, Mw=55 000, from Aldrich) was added into the above solution and the suspension was stirred for 24h to ensure adequate adsorption of PVP on the surface of the  $\text{SiO}_2$ . Unadsorbed PVP components were removed by centrifugation. The

above precipitate was redispersed into 500mL of deionized water via ultrasound. 2ml of pyrrole monomer was afterwards added into the above solution followed with stirring for 5h, after then the oxidant ammonium persulfate (APS) (with a molar ratio to monomer of 1:1) was added into the suspension. The reaction was allowed to proceed for 12h at 4°C, and the resulting product was washed by deionized water, then PPy@ $\text{SiO}_2$  composite was gained. The composite particles were soaked in an aqueous solution of 10 wt% HF for 24 h to remove the silica cores. And then the sample was separated by centrifugation at 10000 rpm for 10 min and washed four times with water and ethanol respectively. Finally, the obtained T-HSSP were dried at 50 °C for 24h in a vacuum oven.

### Preparation of S@PPy composite

Mixture of sulfur and the T-HSSP in the weight ratio of 2:1 was sealed into a glass tube filled with argon and co-heated at 155 °C for 10 h. During the heating process, the sulfur was molten and filled to the holes of the T-HSSP. The mixture was further heated at 300 °C for 6 h to vaporize the sulfur remained on the outside surface of the PPy spheres<sup>34</sup>. The samples are denoted as S@PPy-155 and S@PPy-300, respectively. S@PPy-300 was further heated to 180 °C to remove the sulfur on the outer surface of T-HSSP, then H-S@PPy was obtained. The pure sulfur cathode is prepared by heating the mixture of Acetylene black(AB) and sulfur (weight ratio of 2:1) at 300°C for 6 h.

### Preparation of the sulfur cathode and coin-type Li-S cell

To prepare cathodes, the slurries were prepared by ball milling 80wt% sulfur based composite, 10wt% acetylene black (AB) as conductive agent, both 5wt% CMC, 5wt% SBR as binders and deionized water as the solvent. The slurries were then casted onto an aluminum foil substrate. After the solvent evaporated, the electrodes were cut into circles with 14 mm in diameter and then dried at 60 °C under vacuum for 12 h. CR2025 type coin cells were assembled in a glove box with oxygen and water contents less than 1 ppm. A solution of 1 M LITFSI dissolved in DOL/DME/PYR<sub>14</sub>TFSI (v/v/v= 2/2/1) was employed as the electrolyte. Celgard 2400 was used as the separator and lithium foil as both the counter and reference electrodes.

### Characterization

Elemental analyzer (Tecnai G2 F20) was applied to determine the components of the composite (the average value of more than ten regions). FTIR spectra were carried out on a Thermo Nicolet 7000-C Fourier Transform Spectrometer with  $\pm 2\text{cm}^{-1}$  resolution between 4000 and  $400\text{cm}^{-1}$  using KBr disk method. Specific surface area was tested using the Brunauer-Emmett-Telley (BET) method on a Micromeritics Tristar 3000. SEM images were measured with field emission scanning electron microscope (FESEM JSM-6700) and scanning electron microscope (Hitachi S-3400N). Transmission electron microscopy (TEM) images were measured on a JEOL JEM-2010 transmission electron microscope.

AC impedance measurements were carried out by a Frequency Response Analyzer (FRA) technique on an Autolab Electrochemical Workstation over the frequency range from 0.01Hz to 10 MHz with the amplitude of 10 mV. Cyclic-voltammetry (CV) measurement was also conducted using the Autolab Electrochemical Workstation. The galvanostatic charge and discharge tests were conducted on a LAND CT2001A battery test system in a voltage range of 1.5-2.8 V (vs.  $\text{Li}/\text{Li}^+$ ).

## Results and Discussion

### Structural characterization

Since the T-HSSP are fabricated using SiO<sub>2</sub> as the template. The diameter of T-HSSP and the thickness of the capsules are dependent on the diameter of silica template as well as the weight ratio of [silica spheres template]/[pyrrole monomer]. Fig. 2a, Fig. 2b and Fig. S2 show the TEM and SEM images of the mono-dispersed T-HSSP with diameter of about 300 nm and wall thickness of about 30nm. It is noted that the shell of T-HSSP is composed of a mono layer of PPy nano-particles with diameter in the range of 25-35nm, which supply enough void space to load more sulfur and buffer volume expansion. The heating treatment process successfully combined the sublimed sulfur into the holes of the T-HSSP, which make up a composite with sulfur content as high as 58.4 wt.% as proved by elemental analyzer. No sulfur particles is observed in S@PPy-300 composite, hence, to analyze the distribution of the sulfur in the T-HSSP based composite, elemental mapping and line scan analysis of sulfur in S@PPy-300 composite is carried out. Fig. 2e and Fig. 2f confirm that the sulfur in the composite is uniformly distributed inside the hollow spheres with fractions of it attached on the outer surface.

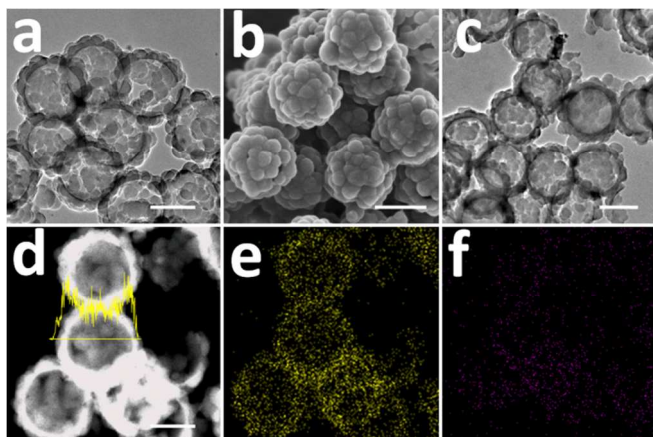


**Fig. 2** (a)TEM image of T-HSSP, (b) SEM image of T-HSSP (c) TEM image of S@PPy-300 composite, (d) STEM image and line scan analysis (sulfur) of S@PPy-300 composite, (e) element mapping of sulfur in (d), (f) element mapping of carbon in (d). All scale bars: 200nm.

Fig.3a shows the XRD patterns of sulfur, T-HSSP, S@PPy-155 and S@PPy-300 composites. As seen, the S@PPy-300 composite displays a very broad reflection peak compared to that of S@PPy-155, indicating amorphous feature of the sulfur generated during heating treatment under higher temperature. And more uniform distribution between sulfur and T-HSSP is obtained after heating treatment under 300°C than 155°C<sup>34, 38, 44</sup>. Moreover, FTIR measurements are further carried out on the T-HSSP and, S@PPy-155 and S@PPy-300 composite to demonstrate a possible structural change of the PPy matrix during the co-heating process with sulfur. As shown in Fig. 3b, the primitive PPy sample exhibits its characteristic bands, involving the pyrrole ring fundamental vibration at 1545cm<sup>-1</sup> and 1458cm<sup>-1</sup>, the C-H in-plane vibration at 1291cm<sup>-1</sup> and 1043cm<sup>-1</sup> and the C-N stretching vibration at 1175cm<sup>-1</sup>. They are consistent with the results reported earlier<sup>34, 53</sup>. FTIR spectrum of S@PPy-155 is consistent with that of T-HSSP, indicating sulfur doesn't react with PPy under the temperature.

However, significant differences are found from the FTIR spectrum of S@PPy-300. The fundamental vibrations of pyrrole ring at 1545cm<sup>-1</sup> and 1458cm<sup>-1</sup> shift obviously to lower wave numbers. The shift is probably attributed to the formation of C-S bond in PPy owing to possible substitution of H atoms on pyrrole ring by S atoms. The C-N stretching vibrational bands at 1175 cm<sup>-1</sup> are therefore also shift to lower wave number. Correspondingly, the intensity of the C-H vibrational band in the vicinity of 1291cm<sup>-1</sup> and 1043cm<sup>-1</sup> is significantly weakened, further confirming the replacement of H atom in aromatic rings by S atom. Moreover, the peak at 1118cm<sup>-1</sup> arose in the heat treated S@PPy-300 composite, which could be assigned to the vibration of C-S bond<sup>54</sup>. Moreover, as shown in Fig.S3, the XPS spectra of S@PPy-300 composite in C 1s region and S 2p region also show the generation of C-S bond during heat treatment<sup>55, 56</sup>. Thus, a possible molecular structure of the S modified PPy is proposed as shown in Fig. 3c where a small amount of elemental sulfur reacts with PPy, and forming a cross-linked stereo PPy-S network with both inter- and/or intra-chain disulfide bond interconnectivity is formed during the heating treatment process, and the rest of the melted elemental sulfur concurrently diffuses into the newly formed polymer network or infuses into the hollow voids. Accordingly, sulfur is both physically and chemically confined in the T-HSSP inhibiting the migration of lithium polysulfides during charge/discharge process. Similar phenomenon was also found in the heated polyaniline-sulfur composite<sup>54, 57</sup>.

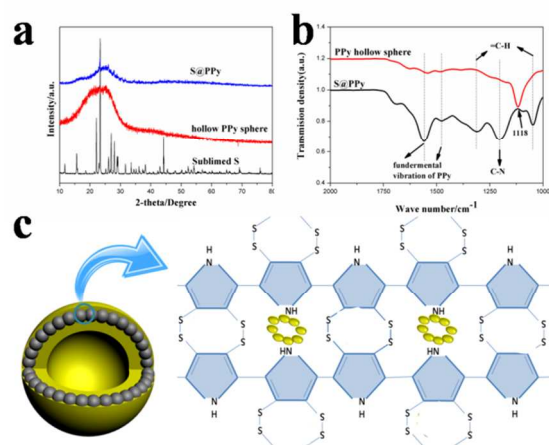


**Fig. 3** (a) the XRD patterns of sublimed S, T-HSSP, S@PPy-155 and S@PPy-300 composite, (b) FTIR spectra of the T-HSSP, S@PPy-155 and S@PPy-300 composite, (c) A possible structure for the S@PPy-300 composite.

### Electrochemical performance

The discharge curves of the S@PPy-300 composite at different rates are shown in Fig. 4a. Two voltage plateaus respectively at about 2.3V and 2.0V are observed. These plateaus are attributed to the reduction of elemental sulfur to higher-order lithium polysulfides (Li<sub>2</sub>S<sub>x</sub>, x≥4), and the reduction of higher-order polysulfides to lower-order polysulfides, respectively<sup>8</sup>. The plateau between 2.3V and 2.0V maybe correspond to the

existence S-C bond<sup>29</sup> (Fig.S4). As demonstrated earlier, besides the holes of T-HSSP to host major of the sulfur, both the inner and outer surface of PPy hollow spheres hold some sulfur. This results into large reaction area, and hence a high utilization rate of sulfur and high discharge specific capacities. As seen, the cells show improved initial discharge capacity as high as 1563.3mAh.g<sup>-1</sup> at 0.2C, 1494.8mAh.g<sup>-1</sup> at 1C, 1320.2mAh.g<sup>-1</sup> at 2C and 1217.3mAh.g<sup>-1</sup> at 5C respectively.

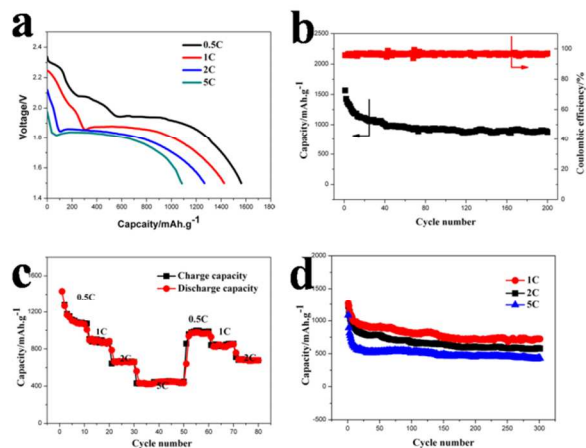


**Fig.4** (a) Initial discharge curves of S@PPy-300 cathode at different rates, (b) the discharge capacity and efficiency coulombic cycling stability of S@PPy-300 cathode at 0.2C, (c) rate performance of S@PPy-300 cathode, (d) cycle life of the S@PPy-300 cathode at 1C, 2C and 5C for long cycles.

The cycling ability and the coulombic efficiency of the S@PPy-300 electrode at 0.2C are shown in Fig.4b. As seen, the discharge specific capacity decreases to about 999.1mAh.g<sup>-1</sup> after 40 cycles, showing an obvious capacity decay during the first 40 cycles. While the reversible capacity retains 892.4 mAh.g<sup>-1</sup> after 200 cycles at 0.2C (the average coulombic efficiency of 96.7%), which is about 89.3% of the discharge capacity at the 40th cycle, showing a good reversibility. Correspondingly, the cycling performances of pure sulfur cathode and S@PPy-155 at 0.2C are displayed in Fig. S5 and Fig. S6 respectively. As shown, the initial discharge capacity and the cycling stability of pure sulfur cathode are much lower than those of S@PPy-300 cathode, showing the enhanced cycling performance is obtained by the designed sulfur cathode. Moreover, the cycling stability of S@PPy-300 is better than that of S@PPy-155, which is attributed to the more uniform distribution of sulfur in the cathode and C-S bond generated under higher heating treatment temperature.

As seen in Fig. 4c, the discharge capacity of S@PPy-300 cathode returns to 1018.5 mAh.g<sup>-1</sup> when the rate decreases from 5C to 0.2C. The long cycling performance of sulfur cathode at different rates is shown in Fig. 4d. Although obvious capacity decay during the first several tens of cycles appears, stable discharge capacities at 1C, 2C and 5C respectively of 717.8 mAh.g<sup>-1</sup>, 582 mAh.g<sup>-1</sup> and 417.1 mAh.g<sup>-1</sup> after 300 charge/discharge cycles which is about 74.6% 78.8% and 83.3% of each corresponding capacity at the 40th cycle. Furthermore, it seems that the capacity fade in the initial 50 cycles is so severe, thus a further heating treatment process is carried out for S@PPy-300 to remove the sulfur on the outer surface of T-HSSP. The sulfur content in H-S@PPy is around 45%, which is smaller than that of S@PPy-300. However, the cycling

performance is further enhanced evidently. As shown in Fig. S7, the severe capacity fade in the initial 50 cycles is suppressed effectively.

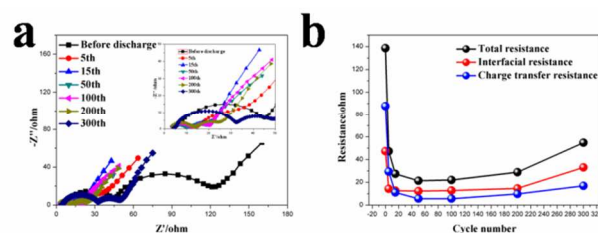
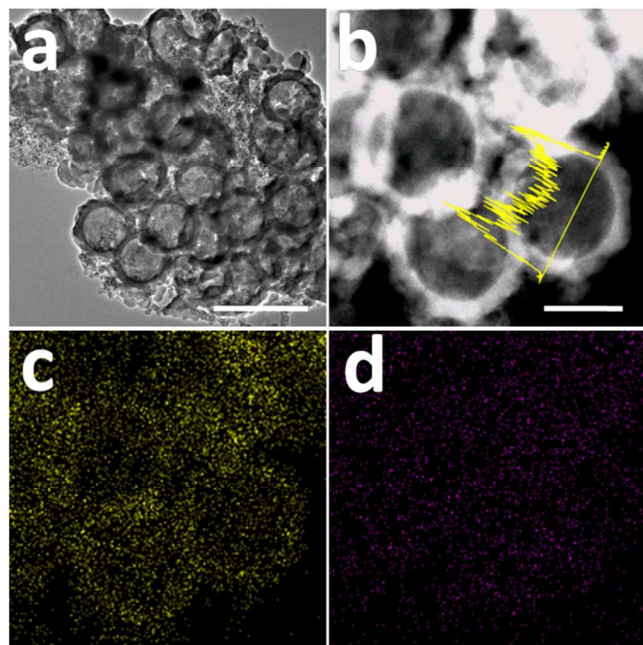


**Fig.5** (a) Electrochemical impedance spectroscopy plots of S@PPy-300 in different cycles after fully charged to 2.8V at 0.5C, (b) The component of the resistance at different cycles.

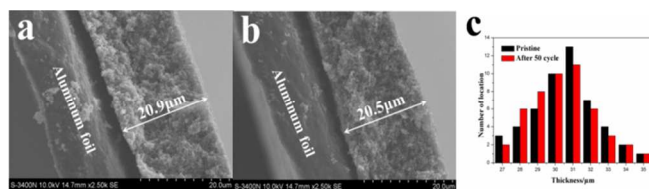
To get further insight into the electrochemical reaction process, electrochemical impedance spectra (EIS) of the S@PPy-300 at the fully charged states for different cycles are measured. Generally, the impedance plots are composed of two semicircles corresponding to the charge transfer impedance and interfacial impedance respectively, and a sloping straight line in the low frequency domain corresponding to the Warburg impedance<sup>58, 59</sup>. Because of the shuttle effect during charge/discharge process, the redistribution of active material is unavoidable, which results in an inhomogeneous distribution of insulating sulfur on the surface of cathode and the corrosion of lithium anode, leading to the increased resistance during charge/discharge process<sup>3</sup>. As shown in Fig.5, the resistance (138.7Ω) before discharge is very high owing to residual insulating sulfur on the outer surface of the T-HSSP. The impedance of the S@PPy-300 sample decreases dramatically to the lowest value (21.4Ω) at the 50th cycle, indicating electrochemical activation and the dissolution of sulfur on the outer surface of T-HSSP during the first tens of cycles. Subsequently, the resistance value rises slightly to 54.9Ω at the 300th cycle, and the interfacial resistance is maintained at around 15Ω between 50cycles and 300cycles, indicating the deposition and aggregation of insulating material on the surface of electrode are not serious in the following cycles for S@PPy-300 cathode.

#### Electrode structural stability

As obtained, S@PPy-300 cathode shows greatly enhanced overall electrochemical performance. In order to deeply understand the mechanism for the enhancement, the morphology of S@PPy-300 cathode after 100 cycles was observed as shown in Fig. 6. As seen, no obvious micro structural change of the cathode appears even after such a long cycling, indicating sufficient mechanical strength of T-HSSP. Furthermore, the elemental analysis results also show the remaining of the uniform distribution of sulfur in T-HSSP after long cycling. The line scan analysis indicates little sulfur on the outer surface of T-HSSP, while almost all of it deposits inside the T-HSSP. Therefore, it is reasonable to explain the serious capacity fading during the first several tens of cycles by the loss of some sulfur weakly trapped on the outer surface of T-HSSP. However, the major sulfur encapsulated inside the T-HSSP is maintained, affording excellent cycling stability during the following cycles.



**Fig. 6** (a) TEM image of S@PPy-300 after 100 cycles at 0.5 C, (b) STEM image of S@PPy-300, elemental mappings of sulfur in (b), and (d) line scan analysis of sulfur in (b). Scale bars: 500nm (a) and 200nm (b).



9. R. Xu, I. Belharouak, J. C. M. Li, X. Zhang, I. Bloom and J. Barenó, *Adv Energy Mater*, 2013, **3**, 833-838.
10. Z. Wei Seh, W. Li, J. J. Cha, G. Zheng, Y. Yang, M. T. McDowell, P.-C. Hsu and Y. Cui, *Nature Communications*, 2013, **4**, 1331-1336.
11. W. Li, G. Zheng, Y. Yang, Z. W. Seh, N. Liu and Y. Cui, *Proceedings of the National Academy of Sciences*, 2013, **110(18)**, 7148-7153.
12. G. C. Li, J. J. Hu, G. R. Li, S. H. Ye and X. P. Gao, *J Power Sources*, 2013, **240**, 598-605.
13. R. Demir-Cakan, M. Morcrette, Gangulibabu, A. Guéguen, R. Dedryvère and J.-M. Tarascon, *Energ Environ Sci*, 2013, **6**, 176-182.
14. L. Suo, Y. S. Hu, H. Li, M. Armand and L. Chen, *Nature Communications*, 2013, **4**, 1481-1488.
15. Z. Jin, K. Xie, X. Hong, Z. Hu and X. Liu, *J Power Sources*, 2012, **218**, 163-167.
16. B. Duan, W. Wang, H. Zhao, A. Wang, M. Wang, K. Yuan, Z. Yu and Y. Yang, *ECS Electrochemistry Letters*, 2013, **2**, A47-A51.
17. Y. M. Lee, N. S. Choi, J. H. Park and J.-K. Park, *J Power Sources*, 2003, **119-121**, 964-972.
18. J. Y. J.L. Wang, J.Y. Xie, N.X. Xu, Y. Li, *Electrochem Commun*, 2002, **4**, 499-502.
19. J. Schuster, G. He, B. Mandlmeier, T. Yim, K. T. Lee, T. Bein and L. F. Nazar, *Angewandte Chemie International Edition*, 2012, **51**, 3591-3595.
20. X. L. Ji, K. T. Lee and L. F. Nazar, *Nat Mater*, 2009, **8**, 500-506.
21. M. Oschatz, S. Thieme, L. Borchardt, M. R. Lohe, T. Biemelt, J. Brückner, H. Althues and S. Kaskel, *Chem Commun*, 2013, **49**, 5832-5834.
22. C. Zhao, L. Liu, H. Zhao, A. Krall, Z. Wen, J. Chen, P. Hurley, J. Jiang and Y. Li, *Nanoscale*, 2014, **6(2)**, 882-888.
23. Y. S. Su and A. Manthiram, *Nature Communications*, 2012, **3**, 1166-1171.
24. B. Zhang, X. Qin, G. R. Li and X. P. Gao, *Energ Environ Sci*, 2010, **3**, 1531-1537.
25. S. Xin, Y.-X. Yin, L. J. Wan and Y.-G. Guo, *Particle & Particle Systems Characterization*, 2013, **30**, 321-325.
26. S. Xin, L. Gu, N.-H. Zhao, Y.-X. Yin, L.-J. Zhou, Y.-G. Guo and L. J. Wan, *J Am Chem Soc*, 2012, **134**, 18510-18513.
27. Z. Zeng, X. Gui, Z. Lin, L. Zhang, Y. Jia, A. Cao, Y. Zhu, R. Xiang, T. Wu and Z. Tang, *Adv Mater*, 2013, **25**, 1185-1191.
28. C. Zu and A. Manthiram, *Adv Energy Mater*, 2013, **3**, 1008-1012.
29. L. Yin, J. Wang, F. Lin, J. Yang and Y. Nuli, *Energ Environ Sci*, 2012, **5**, 6966-6972.
30. T. Lin, Y. Tang, Y. Wang, H. Bi, Z. Liu, F. Q. Huang, X. Xie and M. Jiang, *Energ Environ Sci*, 2013, **6**, 1283-1290.
31. G. Zheng, Q. Zhang, J. J. Cha, Y. Yang, W. Li, Z. W. Seh and Y. Cui, *Nano Lett*, 2013, **13(3)**, 1265-1270.
32. R. Elazari, G. Salitra, A. Garsuch, A. Panchenko and D. Aurbach, *Adv Mater*, 2011, **23**, 5641-5644.
33. J. Li, B. Ding, G. Xu, L. Hou, X. Zhang and C. Yuan, *Nanoscale*, 2013, **5**, 5743-5746.
34. X. Liang, Y. Liu, Z. Wen, L. Huang, X. Wang and H. Zhang, *J Power Sources*, 2011, **196**, 6951-6955.
35. F. Wu, S. X. Wu, R. J. Chen, J. Z. Chen and S. Chen, *Electrochem Solid St*, 2010, **13**, A29-A31.
36. M. Wang, W. Wang, A. Wang, K. Yuan, L. Miao, X. Zhang, Y. Huang, Z. Yu and J. Qiu, *Chem Commun*, 2013, **49**, 10263-10265.
37. L. C. Yin, J. L. Wang, J. Yang and Y. N. Nuli, *J Mater Chem*, 2011, **21**, 6807-6810.
38. N. Jayaprakash, J. Shen, S. S. Moganty, A. Corona and L. A. Archer, *Angewandte Chemie International Edition*, 2011, **50**, 5904-5908.
39. K. Zhang, Q. Zhao, Z. Tao and J. Chen, *Nano Res*, 2012, **6**, 38-46.
40. G. He, S. Evers, X. Liang, M. Cuisinier, A. Garsuch and L. F. Nazar, *Acs Nano*, 2013, **7**, 10920-10930.
41. F. Wu, J. Z. Chen, R. J. Chen, S. X. Wu, L. Li, S. Chen and T. Zhao, *J Phys Chem C*, 2011, **115**, 6057-6063.
42. H. Chen, W. Dong, J. Ge, C. Wang, X. Wu, W. Lu and L. Chen, *Scientific Reports*, 2013, **3**.
43. Y. Fu and A. Manthiram, *Rsc Adv*, 2012, **2**, 5927-5929.
44. Y. Yang, G. Zheng and Y. Cui, *Chem Soc Rev*, 2013, **42**, 3018-3032.
45. Y. Cui, Z. Wen, Y. Lu, M. Wu, X. Liang and J. Jin, *J Power Sources*, 2013, **244**, 614-619.
46. M. Zhou, J. Qian, X. Ai and H. Yang, *Adv Mater*, 2011, **23**, 4913-4917.
47. S. Y. Chew, Z. P. Guo, J. Z. Wang, J. Chen, P. Munroe, S. H. Ng, L. Zhao and H. K. Liu, *Electrochem Commun*, 2007, **9**, 941-946.
48. F. Wu, J. Chen, L. Li, T. Zhao, Z. Liu and R. Chen, *Chemoschem*, 2013, **6**, 1438-1444.
49. Y. Cui, Z. Wen, X. Liang, Y. Lu, J. Jin, M. Wu and X. Wu, *Energ Environ Sci*, 2012, **5**, 7893-7897.
50. Z. Dong, J. Zhang, X. Zhao, J. Tu, Q. Su and G. Du, *Rsc Adv*, 2013, **3**, 24914-24917.
51. Lingyun Hao, C. Zhu, Chunlian Chen, P. Kangb, Yuan Hua, W. F. a and Z. Chenb, *Synthetic Met*, 2003, **139**, 391-396.
52. W. Stöber and A. F. , *J Colloid Interf Sci*, 1968, **8**, 62-69.
53. M. Sun, S. Zhang, T. Jiang, L. Zhang and J. Yu, *Electrochem Commun*, 2008, **10**, 1819-1822.
54. L. Xiao, Y. Cao, J. Xiao, B. Schwenzer, M. H. Engelhard, L. V. Saraf, Z. Nie, G. J. Exarhos and J. Liu, *Adv Mater*, 2012, **24**, 1176-1181.
55. S. Xin, L. Gu, N. H. Zhao, Y. X. Yin, L. J. Zhou, Y. G. Guo and L. J. Wan, *J Am Chem Soc*, 2012, **134**, 18510-18513.
56. Z. Liu, H. Nie, Z. Yang, J. Zhang, Z. Jin, Y. Lu, Z. Xiao and S. Huang, *Nanoscale*, 2013, **5**, 3283-3288.
57. W. Zhou, Y. Yu, H. Chen, F. J. DiSalvo and H. D. Abruña, *J. Am. Chem. Soc.* 2013, **135**, 16736-16743
58. Y. Fu, Y. S. Su, A. Manthiram, *Acs Appl Mater Inter*, 2012, **4**, 6046-6052.
59. G. C. Li, G. R. Li, S. H. Ye and X.-P. Gao, *Adv Energy Mater*, 2012, **2**, 1238-1245.